

## **Electronic Supplementary Information**

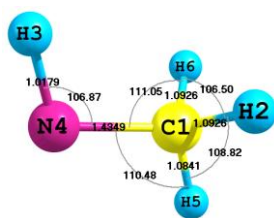
**Hydrogen tunnelling influences the isomerisation of some small radicals of interstellar importance. A theoretical investigation.**

**Tianfang Wang and John H. Bowie**

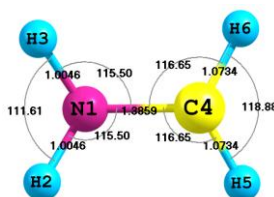
Department of Chemistry, The University of Adelaide, South Australia, 5005.

## Section I Geometric structures and energies.

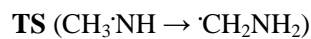
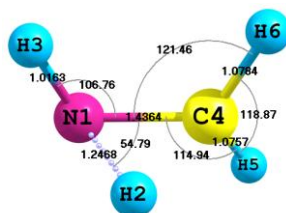
**Fig.S1** Geometries (in Å, deg) of minima and transition state structures optimised at AE-MP2/aug-cc-pVTZ level of theory.



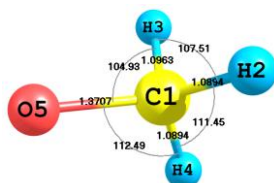
$$\begin{aligned}\tau(2,1,4,3) &= 59.20^\circ \\ \tau(5,1,4,3) &= -179.95^\circ \\ \tau(6,1,4,3) &= -59.11^\circ\end{aligned}$$



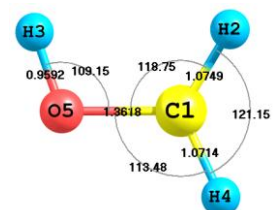
$$\begin{aligned}\tau(3,1,4,2) &= 132.80^\circ \\ \tau(5,4,1,2) &= 39.14^\circ \\ \tau(6,4,1,2) &= -171.94^\circ\end{aligned}$$



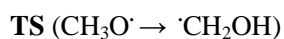
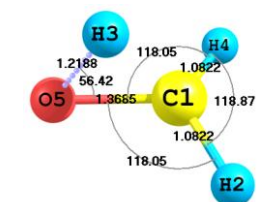
$$\begin{aligned}\tau(2,1,4,3) &= -92.75^\circ \\ \tau(5,4,1,3) &= -170.60^\circ \\ \tau(6,4,1,3) &= -15.27^\circ\end{aligned}$$



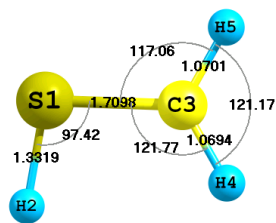
$$\begin{aligned}\tau(3,1,5,2) &= -116.57^\circ \\ \tau(4,1,5,2) &= 126.85^\circ\end{aligned}$$



$$\begin{aligned}\tau(2,1,5,3) &= 22.65^\circ \\ \tau(4,1,5,3) &= 174.48^\circ\end{aligned}$$

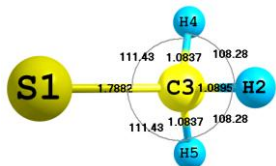


$$\begin{aligned}\tau(3,5,1,2) &= 102.66^\circ \\ \tau(4,1,5,2) &= 154.67^\circ\end{aligned}$$



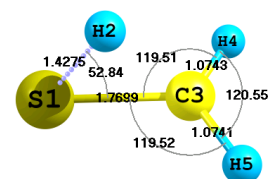
$$\tau(2,1,3,4) = -179.72^\circ$$

$$\tau(5,3,1,4) = -0.27^\circ$$



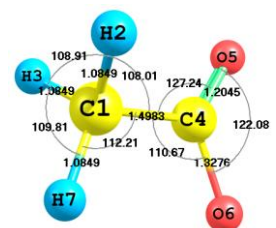
$$\tau(4,3,1,2) = -117.69^\circ$$

$$\tau(5,3,1,2) = 117.68^\circ$$



$$\tau(2,1,3,4) = -93.69^\circ$$

$$\tau(5,3,1,4) = -172.62^\circ$$

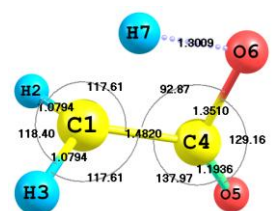
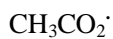


$$\tau(3,1,4,2) = 117.64^\circ$$

$$\tau(5,4,1,2) = -58.80^\circ$$

$$\tau(6,4,1,2) = 121.20^\circ$$

$$\tau(7,1,4,2) = -121.18^\circ$$

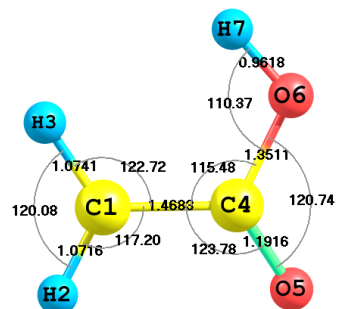
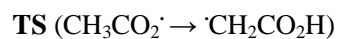


$$\tau(3,1,4,2) = 151.55^\circ$$

$$\tau(5,4,1,2) = -75.77^\circ$$

$$\tau(6,4,1,2) = 104.23^\circ$$

$$\tau(7,1,4,2) = -104.23^\circ$$



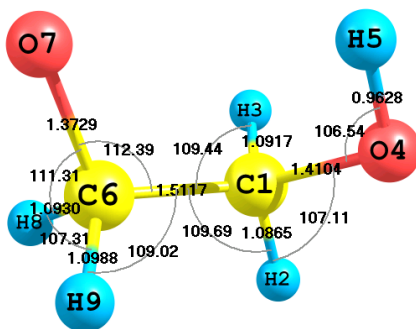
$$\tau(3,1,4,2) = -179.99^\circ$$

$$\tau(5,4,1,2) = 0.01^\circ$$

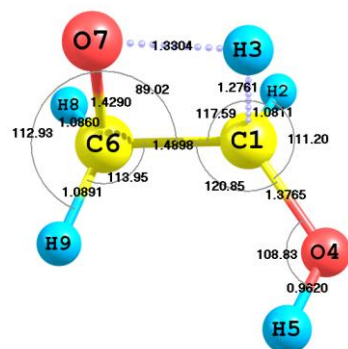
$$\tau(6,4,1,2) = -180.00^\circ$$

$$\tau(7,6,4,1) = 0.01^\circ$$

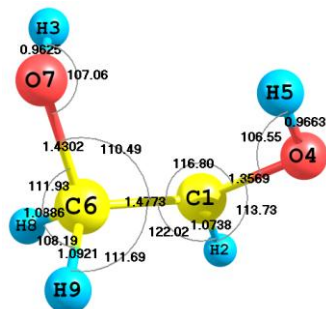




$$\begin{aligned}\tau(3,1,6,2) &= 118.65^\circ \\ \tau(4,1,6,2) &= -118.23^\circ \\ \tau(5,4,1,6) &= -52.25^\circ \\ \tau(7,6,1,2) &= 175.46^\circ \\ \tau(8,6,1,2) &= -57.89^\circ \\ \tau(9,6,1,2) &= 61.09^\circ\end{aligned}$$



$$\begin{aligned}\tau(3,1,6,2) &= 104.45^\circ \\ \tau(4,1,6,2) &= -141.96^\circ \\ \tau(5,4,1,6) &= -26.19^\circ \\ \tau(7,6,1,2) &= -106.41^\circ \\ \tau(8,6,1,2) &= 8.49^\circ \\ \tau(9,6,1,2) &= 138.84^\circ\end{aligned}$$



$$\begin{aligned}\tau(3,7,6,1) &= 64.60^\circ \\ \tau(4,1,6,2) &= -147.95^\circ \\ \tau(5,4,1,6) &= -24.30^\circ \\ \tau(7,6,1,2) &= -163.50^\circ \\ \tau(8,6,1,2) &= -39.17^\circ \\ \tau(9,6,1,2) &= 81.23^\circ\end{aligned}$$

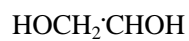


**Table S1** Cartesian coordinates (in Å) of minima and transition state structures, optimised at AE-MP2(full)/aug-cc-pVTZ level of theory.

Methylamino radical (CH <sub>3</sub> NH)			
	X	Y	Z
N1	-0.705303	-0.037298	-0.268670
H2	0.801231	-0.024979	1.183637
H3	-1.167368	0.749779	0.181881
C4	0.680205	0.026308	0.098982
H5	1.230573	-0.790894	-0.353318
H6	1.127588	0.971087	-0.218853

1-amino-methylene (·CH <sub>2</sub> NH <sub>2</sub> )			
	X	Y	Z
N1	-0.646316	-0.068071	-0.004634
H2	-1.002643	-0.801638	0.582044
H3	-1.167413	0.783195	0.109755
C4	0.732324	0.072893	-0.012587
H5	1.308893	-0.832361	0.000848
H6	1.125620	0.930445	-0.524465

TS (CH <sub>3</sub> NH → ·CH <sub>2</sub> NH <sub>2</sub> )			
	X	Y	Z
N1	-0.746312	-0.129803	-0.093598
H2	-0.079861	-0.238417	0.954552
H3	-1.154256	0.794605	0.015269
C4	0.677628	0.031979	0.002998
H5	1.251630	-0.841561	-0.251213
H6	1.140905	1.002122	-0.081411

Methoxy radical (CH <sub>3</sub> O·)			
	X	Y	Z
C1	-0.009339	-0.579370	0.000000
H2	-0.459619	-0.996090	0.900245
H3	1.049987	-0.861876	0.000000
H4	-0.459619	-0.996090	-0.900245
O5	-0.009339	0.791285	0.000000

Hydroxymethyl radical (·CH <sub>2</sub> OH)			
	X	Y	Z
C1	0.682426	0.027401	-0.064974
H2	1.110244	0.985249	0.169286
H3	-1.087482	0.733664	-0.055923
H4	1.226464	-0.879534	0.106606
O5	-0.667973	-0.125473	0.021234

TS (CH <sub>3</sub> O· → ·CH <sub>2</sub> OH)			
	X	Y	Z
C1	0.035099	0.624961	0.000000
H2	0.244458	1.133837	0.931814
H3	-0.980301	-0.069338	0.000000
H4	0.244458	1.133837	0.931814
O5	0.035099	-0.743513	0.000000

Mercaptomethyl radical ( $\cdot\text{CH}_2\text{SH}$ )

	X	Y	Z
S1	-0.413902	-0.508771	0.317039
H2	-0.711494	0.571951	1.036348
C3	1.205118	-0.094573	-0.044361
H4	1.644213	0.816375	0.303337
H5	1.763260	-0.786315	-0.640315

Methylthio radical ( $\text{CH}_3\text{S}\cdot$ )

	X	Y	Z
S1	-0.593665	0.000071	-0.047563
H2	1.413416	-0.001729	1.152988
C3	1.189501	-0.000130	0.086793
H4	1.619490	0.893805	-0.349474
H5	1.619488	-0.892754	-0.352150

TS ( $\cdot\text{CH}_2\text{SH} \rightarrow \text{CH}_3\text{S}\cdot$ )

	X	Y	Z
S1	-0.643464	0.000000	-0.036440
H2	0.226338	-0.001665	1.095434
C3	1.126438	0.000000	-0.048141
H4	1.655228	0.933019	-0.110360
H5	1.655234	-0.932675	-0.113186

Methanecarboxylic radical ( $\text{CH}_3\text{CO}_2\cdot$ )

	X	Y	Z
C1	-1.329669	-0.161044	-0.000039
H2	-1.628308	-0.716953	-0.882548
H3	-1.628383	-0.716218	0.882936
C4	0.165205	-0.060052	0.000003
O5	0.957143	-0.967575	0.000093
O6	0.549115	1.210873	-0.000052
H7	-1.806583	0.813357	-0.000485

Carboxymethyl acid radical ( $\cdot\text{CH}_2\text{CO}_2\text{H}$ )

	X	Y	Z
C1	1.358960	-0.229264	0.000018
H2	2.072362	0.570322	0.000088
H3	1.694069	-1.249787	-0.000223
C4	-0.062343	0.139319	0.000007
O5	-0.455112	1.264292	-0.000011
O6	-0.931167	-0.895451	-0.000011
H7	-0.455900	-1.731595	0.000156

TS ( $\text{CH}_3\text{CO}_2\cdot \rightarrow \cdot\text{CH}_2\text{CO}_2\text{H}$ )

	X	Y	Z
C1	-0.929735	-0.886787	0.000000
H2	-1.426590	-1.128846	0.927163
H3	-1.426590	-1.128846	-0.927163
C4	0.000000	0.267312	0.000000
O5	-0.066155	1.459048	0.000000
O6	1.093189	-0.526416	0.000000
H7	0.215321	-1.486511	0.000000

$\cdot\text{OCH}_2\text{CH}_2\text{OH}$			
	X	Y	Z
C1	0.585179	0.069647	0.637364
H2	1.008669	0.857592	1.254041
H3	0.379201	-0.791414	1.276008
O4	1.543116	-0.245662	-0.348678
H5	1.114546	-0.849453	-0.964106
C6	-0.703433	0.550782	0.010379
O7	-1.235645	-0.367178	-0.860835
H8	-1.439922	0.866271	0.753877
H9	-0.489009	1.419940	-0.626751

$\text{HOCH}_2\cdot\text{CHOH}$			
	X	Y	Z
C1	0.661596	0.293416	0.635289
H2	1.086409	0.883320	1.425626
H3	-1.270671	-1.272265	-0.039782
O4	1.582549	-0.217599	-0.220136
H5	1.089166	-0.654281	-0.926990
C6	-0.678278	0.575500	0.080686
O7	-1.158667	-0.547567	-0.663197
H8	-1.365176	0.860413	0.875634
H9	-0.649675	1.385177	-0.651621

TS ( $\cdot\text{OCH}_2\text{CH}_2\text{OH} \rightarrow \text{HOCH}_2\cdot\text{CHOH}$ )			
	X	Y	Z
C1	0.446506	-0.009392	0.503789
H2	0.632307	0.125779	1.560151
H3	-0.293583	-1.044722	0.410629
O4	1.625096	-0.110235	-0.200132
H5	1.428584	-0.076195	-1.141206
C6	-0.736896	0.680036	-0.082405
O7	-1.403575	-0.581639	-0.158120
H8	-1.245433	1.384804	0.568819
H9	-0.551699	1.121460	-1.060687

**Table S2** Zero-point vibrational energies (ZPVEs, calculated at AE-MP2/aVTZ, in hartree), single-point energies (calculated at AE-MP2/aVTZ, AE-CCSD(T)/aVnZ, n = D, T, Q, AE-CCSD(T)/CBS, in hartree) and relative energies (in kJ mol<sup>-1</sup>).

	CH <sub>3</sub> NH	TS	·CH <sub>2</sub> NH <sub>2</sub>
E <sub>MP2</sub>	-95.02834	-94.96852	-95.04429
aug-cc-pVDZ	-94.95580	-94.89148	-94.96422
aug-cc-pVTZ	-95.07241	-95.01014	-95.08333
aug-cc-pVQZ	-95.12148	-95.05929	-95.13342
E <sub>CBS</sub>	-95.18135	-95.11926	-95.19454
ZPVE	0.04999	0.04663	0.05090
ΔE <sub>MP2+ZPVE</sub>	0	148	-39
ΔE <sub>CBS+ZPVE</sub>	0	155	-32

	CH <sub>3</sub> O·	TS	·CH <sub>2</sub> OH
E <sub>MP2</sub>	-114.87637	-114.82874	-114.89877
aug-cc-pVDZ	-114.78918	-114.73474	-114.80115
aug-cc-pVTZ	-114.91837	-114.86623	-114.93211
aug-cc-pVQZ	-114.97525	-114.92326	-114.99012
E <sub>CBS</sub>	-115.03651	-114.9845495	-115.05263
ZPVE	0.03777	0.03361	0.03798
ΔE <sub>MP2+ZPVE</sub>	0	114	-58
ΔE <sub>CBS+ZPVE</sub>	0	125	-42

	CH <sub>2</sub> SH·	TS	CH <sub>3</sub> S·
E <sub>MP2</sub>	-437.52168	-437.47508	-437.54080
aug-cc-pVDZ	-437.42893	-437.38168	-437.44934
aug-cc-pVTZ	-437.57121	-437.52419	-437.58974
aug-cc-pVQZ	-437.63065	-437.58293	-437.64812
E <sub>CBS</sub>	-437.69420	-437.64561	-437.71051
ZPVE	0.03190	0.03021	0.03637
ΔE <sub>MP2+ZPVE</sub>	0	118	-38
ΔE <sub>CBS+ZPVE</sub>	0	123	-31

	CH <sub>3</sub> CO <sub>2</sub> '	TS	'CH <sub>2</sub> CO <sub>2</sub> H
E <sub>MP2</sub>	-228.08926	-228.04232	-228.10859
aug-cc-pVDZ	-227.89796	-227.84745	-227.90931
aug-cc-pVTZ	-228.14900	-228.10040	-228.16204
aug-cc-pVQZ	-228.20626	-228.15735	-228.21928
E <sub>CBS</sub>	-228.26029	-228.21088	-228.27318
ZPVE	0.04863	0.04436	0.04927
ΔE <sub>MP2+ZPVE</sub>	0	112	-49
ΔE <sub>CBS+ZPVE</sub>	0	119	-32

	'OCH <sub>2</sub> CH <sub>2</sub> OH	TS	HOCH <sub>2</sub> 'CHOH
E <sub>MP2</sub>	-229.26374	-229.21469	-229.28965
aug-cc-pVDZ	-229.07313	-229.02399	-229.08859
aug-cc-pVTZ	-229.33190	-229.28394	-229.34915
aug-cc-pVQZ	-229.39409	-229.34585	-229.41137
E <sub>CBS</sub>	-229.45363	-229.40499	-229.47084
ZPVE	0.07279	0.06871	0.07320
ΔE <sub>MP2+ZPVE</sub>	0	118	-67
ΔE <sub>CBS+ZPVE</sub>	0	117	-44

**Table S3** Theoretical and experimental vibrational frequencies of minima in different isomerisations

	Vib. Sym.	Approx. type of mode	$\omega^a$ (cm <sup>-1</sup> )	Expt. (cm <sup>-1</sup> )
CH <sub>3</sub> NH		CH <sub>3</sub> s-deform.	1390	1379 <sup>1</sup>
		CN stretch	1046	1105 <sup>1</sup>
·CH <sub>2</sub> NH <sub>2</sub>	<i>a'</i>	NH <sub>2</sub> scissors	1665	1700 <sup>2</sup>
		Deformation	622	600 <sup>2</sup>
CH <sub>3</sub> O·	<i>a''</i>	CH <sub>3</sub> stretch	2880	2840 <sup>3,4</sup>
		CO stretch	1025	1047 <sup>3,4</sup>
		HCO deform.	671	651.5 <sup>3-5</sup>
	<i>a'</i>	CH <sub>3</sub> stretch	2960	2955 <sup>6</sup>
		CH <sub>3</sub> stretch	2900	2885 <sup>7,8</sup>
		CH <sub>2</sub> scissors	1398	1406±2 <sup>9</sup>
		Umbrella	1370	1376 <sup>6</sup>
		HCO deform.	1398	1233 <sup>6,10,11</sup>
·CH <sub>2</sub> OH	<i>a'</i>	OH stretch	3698	3674.9 <sup>12</sup>
		CH <sub>2</sub> a-stretch	3230	3161.5 <sup>12</sup>
		CH <sub>2</sub> s-stretch	3150	3043.4 <sup>12</sup>
		CH <sub>2</sub> scissors	1504	1459 <sup>13</sup>
	<i>a</i>	OH deform.	1330	1334 <sup>13,14</sup>
		CO stretch	1222	1183 <sup>13,14</sup>
		HCOH deform.	1048	1048 <sup>13,14</sup>
		Torsion	429	420 <sup>13,14</sup>
		H <sub>2</sub> CO OPLA	177	234±5 <sup>15</sup>
CH <sub>3</sub> S·	<i>a</i> <sub>1</sub>	CH <sub>3</sub> stretch	3004	2960±30 <sup>16</sup>
		Umbrella	1321	1313±5 <sup>17,18</sup>
		CS stretch	753	727±3 <sup>16-18</sup>
	<i>e</i>	CH <sub>3</sub> deform.	1458	1496±6 <sup>17</sup>
·CH <sub>2</sub> SH		H <sub>2</sub> CS umbrella	434	425 <sup>19,20</sup>

<sup>a</sup>Calculated at AE-MP2/aVTZ level of theory.

## Section II Tunnelling effects estimated by Eckart method

### 1. Eckart tunnelling analysis

For Eckart method, the cross-section of the potential energy surface is fitted with the Eckart potential,<sup>21-23</sup>

$$V(s) = \frac{A \exp(\frac{s-s_0}{L})}{1 + \exp(\frac{s-s_0}{L})} + \frac{B \exp(\frac{s-s_0}{L})}{[1 + \exp(\frac{s-s_0}{L})]^2} \quad (s1)$$

The fitting parameters are

$$A = V_r - V_f$$

$$B = (\sqrt{V_r} + \sqrt{V_f})^2$$

$$L = \frac{2\pi}{\omega^*} \sqrt{\frac{2}{\mu}} \left( \frac{1}{\sqrt{V_r}} + \frac{1}{\sqrt{V_f}} \right)^{-1}$$

where  $V_f$  and  $V_r$  are the energy barriers with ZPEs (excluding the vibration corresponding to the reaction mode) in the forward and reverse direction,  $\omega^*$  is the absolute value of imaginary frequency of the transition state. Hence, the transmission probability as a function of energy is

$$P(\varepsilon) = \frac{\cosh(\alpha + \beta) - \cosh(\alpha - \beta)}{\cosh(\alpha + \beta) + \cosh \delta} \quad (s2)$$

The parameters are

$$\alpha = \frac{4\pi}{\hbar\omega^*} \left( \frac{1}{\sqrt{V_r}} + \frac{1}{\sqrt{V_f}} \right)^{-1} \sqrt{\varepsilon}$$

$$\beta = \frac{4\pi}{\hbar\omega^*} \left( \frac{1}{\sqrt{V_r}} + \frac{1}{\sqrt{V_f}} \right)^{-1} \sqrt{\varepsilon - V_r + V_f}$$

$$\delta = 4\pi \sqrt{\frac{V_r V_f}{(\hbar\omega^*)^2} - \frac{1}{16}}$$

where  $\varepsilon$  is the collision energy. The rate constant can be calculated by the following equation,

$$k_{Eckart} = \frac{\omega_0}{2\pi} P(\varepsilon) = \frac{\omega_0}{2\pi} \frac{\cosh(\alpha + \beta) - \cosh(\alpha - \beta)}{\cosh(\alpha + \beta) + \cosh \delta} \quad (s3)$$

Eventually, the temperature dependant rate constant expression for Eckart methods is similar to that of WKB [eqn (4) in the text],

## 2. Results and discussion

**Table S4** Key parameters used in Eckart estimation

Isomerisation	$\omega^*$ (cm <sup>-1</sup> )	$V_r$ (cm <sup>-1</sup> )	$V_f$ (cm <sup>-1</sup> )	$\omega_{0,\text{forward}}$ (cm <sup>-1</sup> )	$\omega_{0,\text{reverse}}$ (cm <sup>-1</sup> )
$\cdot\text{CH}_2\text{SH} \rightarrow \text{CH}_3\text{S}\cdot$	1688.4	8010.5	12945.5	820.7	755.3
$\text{CH}_3\text{O}\cdot \rightarrow \cdot\text{CH}_2\text{OH}$	2122.2	10426.5	12437.8	978.2	1116.1
$\text{CH}_3\text{CO}_2\cdot \rightarrow \cdot\text{CH}_2\text{CO}_2\text{H}$	2308.6	9838.0	11213.8	368.9	327.9
$\text{HOCH}_2\text{CH}_2\text{O}\cdot \rightarrow \text{HO}\cdot\text{CHCH}_2\text{OH}$	2243.0	9629.6	13031.4	528.5	547.8
$\text{CH}_3\cdot\text{NH} \rightarrow \cdot\text{CH}_2\text{NH}_2$	2108.3	12823.2	15333.2	985.7	663.9

### 2.1 $\text{CH}_3\cdot\text{NH}$ and $\cdot\text{CH}_2\text{NH}_2$

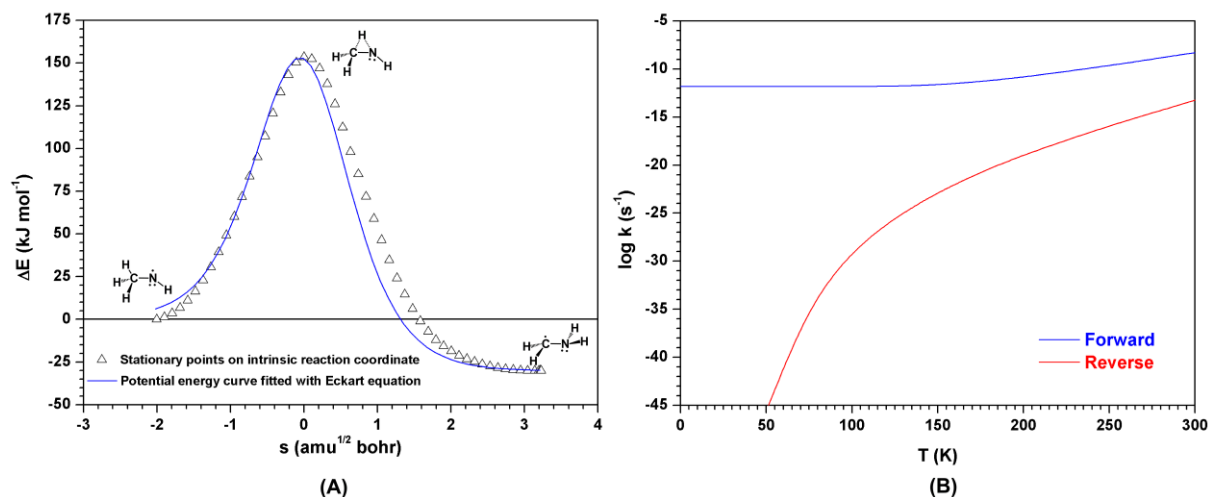


**Fig.S2** Potential energy curve and rate constants for the isomerisation of  $\text{CH}_3\cdot\text{NH}$  to  $\cdot\text{CH}_2\text{NH}_2$ . (a) Along the intrinsic reaction coordinate (open triangles), the geometric structures and zero-point vibrational corrections were calculated at AE-MP2/aVTZ level of theory. Final energies were determined from AE-CCSD(T)/aVQZ single points at the stationary points. The blue curve is the Eckart fitting of the potential. (b) Temperature dependence of Eckart tunnelling corrected rate constants for forward and reverse reactions.

The results of the Eckart method is shown in Figure S2a, and it is clear that the Eckart potential behaves well in the reverse direction (reverse from TS) of the reaction coordinate, though certain errors emerge at the region of positive  $s$  values. As it narrows the width of the barrier that the reactant  $\text{CH}_3\cdot\text{NH}$  ‘penetrates’, the transmission probability would be different from the value calculated from the IRC, in this case, an increase is observed. This means that the rate constants increase accordingly, illustrated in Figure

S2b, i.e.,  $k_{\text{Eckart}}$  is nearly 1.5 orders of magnitude higher than  $k_{\text{WKB}}$  at the zero limit. This discrepancy decreases gradually as the temperature increases, to  $\sim 1$  order of magnitude at 300K. Moreover, the relationship between the rate constants (both forward and reverse) and temperature show similar trends for both WKB and Eckart methods.

## 2.2 $\text{CH}_3\text{O}^\cdot$ and $^\cdot\text{CH}_2\text{OH}$

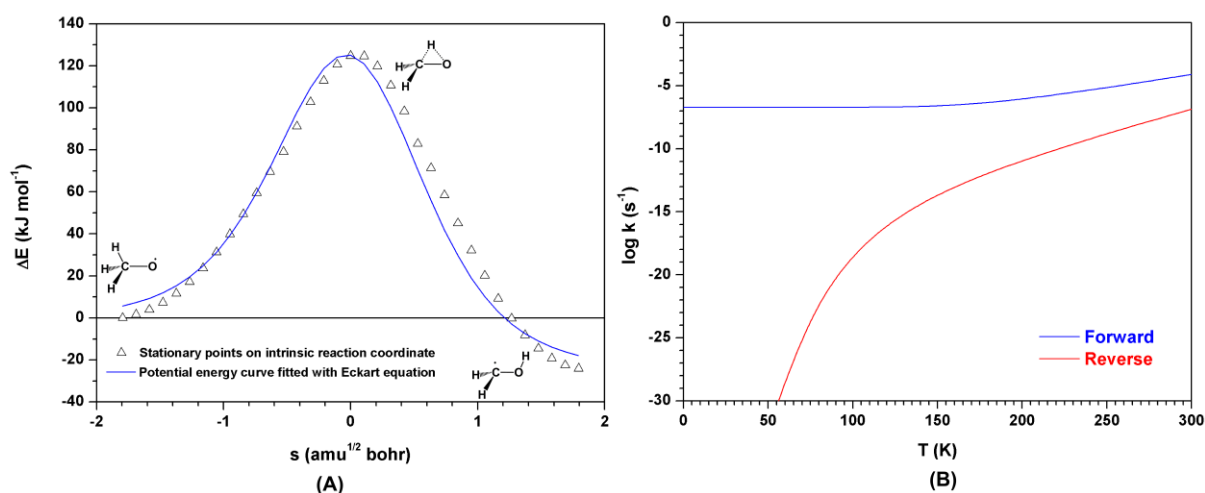


**Fig.S3** Potential energy curve and rate constants for the isomerisation of  $\text{CH}_3\text{O}^\cdot$  to  $^\cdot\text{CH}_2\text{OH}$ . (a) Along the intrinsic reaction coordinate (open triangles), the geometric structures and zero-point vibrational corrections were calculated at AE-MP2/aVTZ level of theory, and final energetics were determined from AE-CCSD(T)/aVQZ single points at the stationary points. The blue curve is the Eckart fitting of the potential; (b) temperature dependence of Eckart tunnelling corrected rate constants for forward and reverse reactions.

The Eckart potential narrows the barrier width; moreover, its tail decreases slower than the intrinsic reaction coordinate, with the consequence that  $k_{\text{Eckart}}$  is about 0.5 order of magnitude higher than  $k_{\text{WKB}}$  with this discrepancy diminishing. Both methods show a significant increase of rate constant above 200K, giving a half-life of 2.41 (Eckart) and 14.64 (WKB) hr at room temperature, respectively.

### 2.3 $\cdot\text{CH}_2\text{SH}$ and $\text{CH}_3\text{S}\cdot$

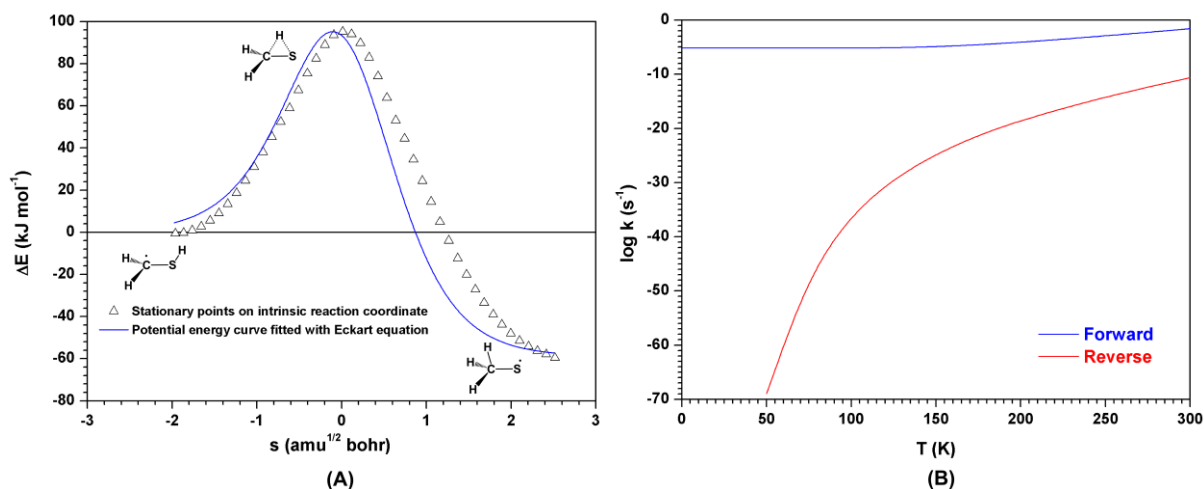


**Fig.S4** Potential energy curve and rate constants for the isomerisation of  $\cdot\text{CH}_2\text{SH}$  to  $\text{CH}_3\text{S}\cdot$ : (a) Along the intrinsic reaction coordinate (open triangles), the geometric structures and zero-point vibrational corrections were calculated at AE-MP2/aVTZ level of theory; final energies were determined from AE-CCSD(T)/aVQZ single points at the stationary points. The blue curve is the Eckart fitting of the potential; (b) temperature dependence of Eckart tunnelling corrected rate constants for forward and reverse reactions.

### 2.4 $\text{CH}_3\text{CO}_2\cdot$ and $\cdot\text{CH}_2\text{CO}_2\text{H}$

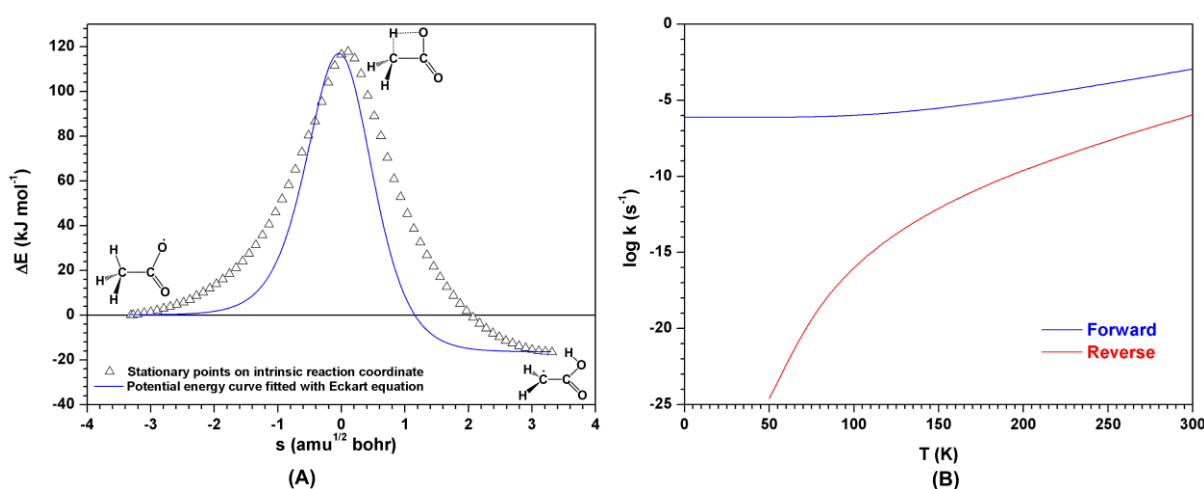


**Fig.S5** Potential energy curve and rate constants for the isomerisation of  $\text{CH}_3\text{CO}_2\cdot$  to  $\cdot\text{CH}_2\text{CO}_2\text{H}$ . (a) Along the intrinsic reaction coordinate (open triangles), the geometric structures and zero-point vibrational corrections were calculated at AE-MP2/aVTZ level of theory; final energies were determined from

AE-CCSD(T)/aVTZ single points at the stationary points. The blue curve is the Eckart fitting of the potential; (b) temperature dependence of Eckart tunnelling corrected rate constants for forward and reverse reactions.

### 2.5 HOCH<sub>2</sub>CH<sub>2</sub>O<sup>•</sup> and HO<sup>•</sup>CHCH<sub>2</sub>OH

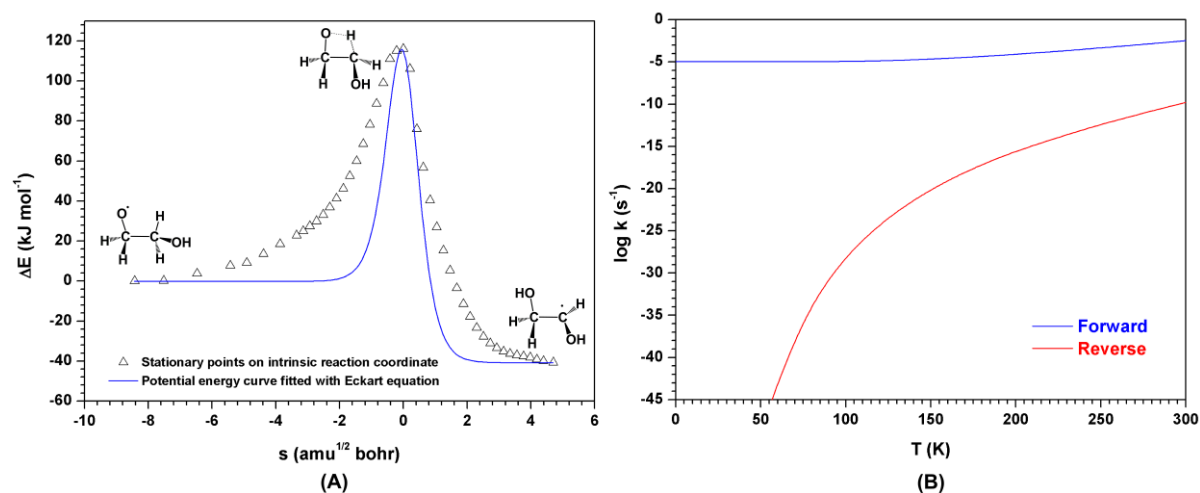


**Fig.S6** Potential energy curve and rate constants for the isomerisation of HOCH<sub>2</sub>CH<sub>2</sub>O<sup>•</sup> to HO<sup>•</sup>CHCH<sub>2</sub>OH. (a) Along the intrinsic reaction coordinate (open triangles), the geometric structures and zero-point vibrational corrections were calculated at AE-MP2/aVTZ level of theory. Final energies were determined from AE-CCSD(T)/aVTZ single points at the stationary points. The blue curve is the Eckart fitting of the potential; (b) temperature dependence of Eckart tunnelling corrected rate constants for forward and reverse reactions.

The tunnelling effects evaluated by the Eckart method are displayed in Figures S2-S6. It is clear that in the cases of CH<sub>3</sub><sup>•</sup>NH, CH<sub>3</sub>O<sup>•</sup> and <sup>•</sup>CH<sub>2</sub>SH, the Eckart potential represents the potential energy surface within a reasonable error range, usually narrowing the barrier significantly at the bottom of the barrier. Thus the Eckart tunnelling corrected rate constants are higher at low temperature, though comparable to those obtained by WKB method as temperature increases. As temperature increases, the results of these two methods should coincide with each other; the narrower the potential energy surface, the better this coincidence becomes. However, for the isomerisations of CH<sub>3</sub>CO<sub>2</sub><sup>•</sup> to <sup>•</sup>CH<sub>2</sub>CO<sub>2</sub>H and HOCH<sub>2</sub>CH<sub>2</sub>O<sup>•</sup> to HO<sup>•</sup>CHCH<sub>2</sub>OH, the Eckart potential does not provide a good fitting to the potential energy surface. This results in large and incorrect transmission probabilities, leading to high tunnelling corrected rate constants

for both forward and reverse directions within the entire temperature range. This is particularly noticeable at low temperature. Therefore, the Eckart method is only applicable to those studied systems when the isomerisation involves a 1, 2 hydrogen transfer.

#### References for supplementary section.

1. D. Radisic, S. J. Xu and K. H. Bowen, *Chem. Phys. Lett.*, 2002, **354**, 9.
2. T. L. Jansen, I. Trabjerg, S. Rettrup, P. Pagsberg and A. Sillesen, *Acta Chem. Scand.*, 1999, **53**, 1054.
3. S. C. Foster, P. Misra, T. Y. D. Lin, C. P. Damo, C. C. Carter and T. A. Miller, *J. Phys. Chem.*, 1988, **92**, 5914.
4. Y. Y. Lee, G. H. Wann and Y. P. Lee, *J. Chem. Phys.*, 1993, **99**, 9465.
5. A. Geers, J. Kappert, F. Temps and T. J. Sears, *J. Chem. Phys.*, 1993, **98**, 4297.
6. M. J. Nee, A. Osterwalder, J. Zhou and D. M. Neumark, *J. Chem. Phys.*, 2006, **125**.
7. J. X. Han, S. M. Hu, H. B. Chen, Y. Utkin, J. M. Brown and R. F. Curl, *Phys. Chem. Chem. Phys.*, 2007, **9**, 3725.
8. J. X. Han, Y. G. Utkin, H. B. Chen, L. A. Burns and R. F. Curl, *J. Chem. Phys.*, 2002, **117**, 6538.
9. S. Y. Chiang, Y. C. Hsu and Y. P. Lee, *J. Chem. Phys.*, 1989, **90**, 81.
10. D. L. Osborn, D. J. Leahy, E. H. Kim, E. de Beer and D. M. Neumark, *Chem. Phys. Lett.*, 1998, **292**, 651.
11. T. M. Ramond, G. E. Davico, R. L. Schwartz and W. C. Lineberger, *J. Chem. Phys.*, 2000, **112**, 1158.
12. L. Feng, J. Wei and H. Reisler, *J. Phys. Chem. A*, 2004, **108**, 7903.
13. M. E. Jacox, *Chem. Phys.*, 1981, **59**, 213.
14. M. E. Jacox and D. E. Milligan, *J. Mol. Spect.*, 1973, **47**, 148.
15. R. D. Johnson and J. W. Hudgens, *J. Phys. Chem.*, 1996, **100**, 19874.
16. R. L. Schwartz, G. E. Davico and W. C. Lineberger, *J. Elect. Spect. & Rel. Phen.*, 2000, **108**, 163.
17. S. Y. Chiang and Y. P. Lee, *J. Chem. Phys.*, 1991, **95**, 66.
18. M. Suzuki, G. Inoue and H. Akimoto, *J. Chem. Phys.*, 1984, **81**, 5405.
19. M. E. Jacox, *Can. J. Chem.*, 1983, **61**, 1036.
20. M. E. Jacox and D. E. Milligan, *J. Mol. Spect.*, 1975, **58**, 142.
21. C. Eckart, *Phys. Rev.*, 1930, **35**, 1303.
22. H. S. Johnston and J. Heicklen, *J. Phys. Chem.*, 1962, **66**, 532.
23. T. N. Truong and D. G. Truhlar, *J. Chem. Phys.*, 1990, **93**, 1761.